

ISSN: 2278-5213

### RESEARCH ARTICLE

Effect of Hall Currents, Chemical Reaction, Heat Source and Forchheimir Parameters on Steady MHD rotating Nanofluid through Non-Darcy Porous Medium over Exponentially Stretching Porous Sheet

### Y. Madhusudhana Reddy

Department of Mathematics, Sri Venkateswara Institute of Technology, Anantapuramu, A.P., India ymsmadhu@gmail.com

### **Abstract**

We explore the influence of Hall currents, rotation, chemical reaction and dissipation on non-Darcy convective heat and mass transfer flow of nanofluids through a porous medium past an exponentially stretching sheet. By using Runge-Kutta–Shooting method the equations have been evaluated for different variations. It is found that the linear and rotational velocities, nanoparticle volume fraction enhance with Hall pall parameter (m) and reduces with rotation parameter (R) while the temperature reduces with m and increases with R. Higher dissipation larger the velocities, temperature and smaller nanoparticle volume fraction.

**Keywords:** Hall currents, rotation, chemical reaction, dissipation, non-darcy porous medium.

### Introduction

The fluid dynamics due to a stretching sheet are important from theoretical as well as practical point of view because of their various applications to polymer technology and metallurgy, During many mechanical forming processes, such as extrusion, melt-spinning, cooling of a large metallic plate in a bath, manufacture of plastic and rubber sheets, glass blowing, continuous casting, and spinning of fibers, the extruded material issues through a die. Provoked by the process of polymer extrusion in which extradite emerges from a narrow slit, first analyzed the two-dimensional fluid flow over a linearly stretching surface. Crane (1970) first studied the boundary layer flow due to linearly stretching sheet. Magyari and Keller (1999) considered the boundary layer flow and heat and mass transfer due to an exponentially stretching sheet. Bhattacharya and Pop (2011) showed the effect of external magnetic field on the flow over an exponentially shrinking sheet. In recent years studies on nanofluids heat and mass transfer boundary layer laminar flow have attracted considerable attention. Choi (1995) introduced the technique of nanofluids by using a mixture of nanoparticles and the base fluids. The presence of the nanoparticles in the nanofluids increases the thermal conductivity and causes significant change in properties such as viscosity and specific heat in comparison to the base fluid. It has attracted many researchers to perform its engineering applications. (2013)Shatevi and Marewo numerically investigated the MHD boundary layer flow with

heat and mass transfer of an incompressible upper-convected Maxwell fluid over a stretching sheet. Ibrahim et al. (2013) analysed numerically the mass transfer and thermal radiation on a steady two-dimensional laminar flow of a viscous incompressible electrically conducting micropolar fluid past a stretching surface embedded in a non-Darcian porous medium in the presence of heat generation. Nandy (2013) investigated the MHD boundary layer flow and heat transfer of a non-Newtonian Casson fluid in the neighbourhood of a stagnation point over a stretching surface in the presence of velocity and thermal slips at the boundary. Khan and Pop (2013) numerically studied steady boundary layer flow past a stretching wedge with the velocity uw[x] in a nanofluids and with a parallel free stream velocity u<sub>e</sub>(x). Njane and Daniel (2013) studied the effect of magnetic field on boundary layer flow of incompressible electrically conducting water-based nanofluids past convectively heated vertical porous plate with Navier slip boundary condition. Goval and Rama Bhargava (2013) analysed the effect of velocity slip boundary condition on the flow and heat transfer of Non-Newtonian nanofluids over a stretching sheet with a heat source/sink, under the action of a uniform magnetic field, oriented normally to the plate. Bhattacharya and Pop (2011) presented a mathematical model of the steady boundary layer flow of a nanofluids due to an exponentially permeable stretching sheet with external magnetic field.



Noghrehabad et al. (2012) examined the combined effects of Brownian motion, thermophoresis, and magnetic field on the steady boundary layer flow and heat transfer of nanofluids over a linear isothermal stretching sheet. Poornima and Reddy (2013) presented a non-linear stretching sheet in the presence of transverse magnetic field. Malvandi et al. (2013) dealt with the steady two-dimensional stagnation point flow of nanofluid towards an exponentially stretching sheet with non-uniform heat generation/absorption. Ferdows et al. (2012) studied MHD boundary layer flow of nanofluids over an exponentially stretching sheet. Hamad and Ferdows (2012) analyzed the boundary layer flow and heat transfer in a viscous fluid containing metallic nanoparticles over a non-linear stretching sheet. Khan et al. (2011) investigated numerically the study of MHD radiative heat transfer in a nanofluid within the influence of magnetic field over a stretching surface. Takhar et al. (2012) studied the flow and heat transfer on a stretching surface in a rotating fluid in the presence of a magnetic field. In this study, we analyze the effect of Hall currents and rotation on the non-Darcy convective heat and mass transfer flow of a nanofluid through a porous medium past a porous exponentially stretching surface under the influence of magnetic field. The non-linear governing equations have been solved by fourth order Runge-Kutta-shooting technique. The velocity, rotational velocity, temperature and nanoparticle volume fraction have been discussed graphically for different variations of governing parameters. The skin friction, rate of heat and mass transfer on the wall has been evaluated numerically for different variations.

### 2. Formulation of the Problem

We consider the steady boundary layer flow with rotational (angular) motion over a stretching surface in a porous medium filled with nanofluids. A uniform magnetic field is applied normal to the plate. Assuming the magnetic Reynolds number to be small we neglect the induced magnetic field. The fluid is assumed to be electrically conducting, the convecting fluid and the porous medium are everywhere in thermodynamic equilibrium. It is assumed that the uniform temperature of the surface is Tw and that of the nanofluids volume fraction is Cw, the uniform temperature and nanofluids volume fraction in the ambient(free flow region) fluid are  $T_{\infty}$  and  $T_{\infty}$  respectively. There is no rotational motion of the ambient (free flow region) fluid.

It is also assumed that the plate is exponentially stretched with a velocity  $u_w(x) = c \exp(\frac{x}{L})$ , where c is a

positive constant and having no initial rotational motion. The flow is assumed to be high so that an advective term and a Forchheimer quadratic drag term do appear in the momentum equations. The viscous dissipation and radiation terms have not been taken into account.

A uniform strong magnetic field of strength B<sub>0</sub> is imposed along the y-axis and the effect of Hall current is taken into account. Taking Hall effects into account the generalized Ohm's law provided in the following form

$$\vec{J} = \frac{\sigma}{1 + m^2} (\vec{E} + \vec{V} * + \vec{B} - \frac{1}{en_e} \vec{f} * \vec{B})$$

Where  $m = \frac{\sigma B_o}{e n_c}$  is defined as the Hall current parameter. A very interesting fact that the effect of Hall

current gives rise to a force in the z-direction which in turn produces a cross-flow velocity in this direction and then the flow becomes three-dimensional.

Under these assumptions, the following five field equations embodying the conservation of total mass, momentum (Brinkman-Forchheimer equations), energy and nanofluids volume fraction equations for the nanofluids are considered as follows:

The equation of continuity:

$$\frac{\partial u}{\partial x} + \frac{\partial v}{\partial y} = 0 \tag{1}$$

The momentum equations:



Volume 2, Issue 12 May 2014

$$u\frac{\partial u}{\partial x} + v\frac{\partial u}{\partial y} = \left(\frac{\mu}{\rho_f}\right)\frac{\partial^2 u}{\partial y^2} - \frac{\sigma\mu_e^2 B^2}{\rho_f}(u + mw) - \left(\frac{\mu}{k}\right)u - \frac{b}{\sqrt{k}}u^2 + 2\Omega w + \beta g(T - T\infty) + \beta^* g(C - C_\infty)$$
(2)

$$u\frac{\partial w}{\partial x} + v\frac{\partial w}{\partial y} = \left(\frac{\mu}{\rho_f}\right)\frac{\partial^2 w}{\partial y^2} + \frac{\sigma\mu_e^2 B^2}{\rho_f}(mu - w) - \left(\frac{\mu}{k}\right)w - \frac{b}{\sqrt{k}}w^2 - 2\Omega u \tag{3}$$

The equation of Energy:

$$u\frac{\partial T}{\partial x} + v\frac{\partial T}{\partial y} = k_f \frac{\partial^2 T}{\partial y^2} - \frac{Q_H}{\rho C_p} (T - T_{\infty}) + \frac{v}{C_p} ((\frac{\partial u}{\partial y})^2 + (\frac{\partial w}{\partial y})^2) + \frac{\sigma B_o^2}{\rho (1 + m^2)} (u^2 + w^2) + \frac{(\rho C)_p}{(\rho C)_f} (D_B \frac{\partial T}{\partial y} \frac{\partial C}{\partial y} + \frac{D_T}{T_{\infty}} ((\frac{\partial T}{\partial y})^2)$$

$$(4)$$

The equation of Mass:

$$u\frac{\partial C}{\partial x} + v\frac{\partial C}{\partial y} = D_B \frac{\partial^2 C}{\partial y^2} + \frac{D_T}{T_{\infty}} (\frac{\partial^2 T}{\partial y^2}) - kc(C - C_{\infty})$$
(5)

Where x and y are Cartesian coordinates along the stretching wall and normal to it respectively. u and v are the velocity components along the x-axis and y-axis and w being rotational velocity about normal to x-y plane i.e. about z-

axis. T is the temperature in the fluid phase. C is the nanoparticle volume fraction.  $B(x) = B_0 \exp(\frac{x}{L})$  is variable

magnetic field and  $B_0$  is constant, k is the permeability of the porous medium, b is Forchheimer coefficient,  $\Omega$  is coefficient of rotational motion.  $\rho$ ,  $\nu$  and  $\mu$  are the density, kinematic viscosity and dynamic viscosity of the fluid, respectively. Further,  $(\rho C_p)_f$  is the heat capacity of the fluid,  $(\rho C_p)_p$  is the effective heat capacity of the nanoparticle material and  $k_f$  is the effective thermal conductivity of the porous medium. The coefficient that appears in (2.4) and (2.5) are the source coefficient  $Q_H$ , the Brownian diffusion coefficient  $D_B$  and the thermophoretic diffusion coefficient  $D_T$ . The boundary conditions relevant to the problem are

$$y = 0 : u = u_w(x) = c \exp(\frac{x}{L}), v = v_w, w(x, 0) = 0$$

$$T = T_w = T_\infty + T_o \exp(\frac{x}{L}), C = C_w = C_\infty + C_o \exp(\frac{x}{L})$$

$$y \to \infty : u \to 0, w(x, y) \to 0, T \to T_\infty, C \to C_\infty,$$

$$where \ u_w(x) = c \exp(\frac{x}{L}), v_w(x) = c \exp(\frac{x}{2L})$$

$$(6)$$

Introducing the non-dimensional variables as

$$\eta = \left(\frac{c}{2\nu L}\right)e^{\frac{x}{2L}}y; \psi = (2\nu Lc)^{1/2}e^{\frac{x}{2L}}f(\eta), \theta(\eta) = \frac{T - T_{\infty}}{T_{w} - T_{\infty}};$$

$$\phi(\eta) = \frac{C - C_{\infty}}{C_{w} - C_{\infty}}; u = \frac{\partial \psi}{\partial \eta}; v = -\frac{\partial \psi}{\partial x}; w(x, y) = ce^{\frac{x}{L}}g(\eta)$$
(7)

Here  $\eta$  is similarity variable,  $\psi$  is the stream function,  $\theta$  is non-dimensional temperature,  $\phi$  is the non-dimensional nanoparticle volume fraction.

Using (7) and Rossel and approximation (\*) in equation (4), the governing equations reduces to

$$f''' + ff'' - 2(f')^{2} - \frac{M^{2}}{1 + m^{2}} (f' + mg_{0}) - D^{-1}f' + Fs(f')^{2}$$

$$+ R1g_{0} + G(\theta + N\phi) = 0$$
(8)



$$g_0 + fg_0 - 2fg_0 - R1f' + \frac{M^2}{1 + m^2} (mf' - g_0) - D^{-1}g_0 + Fs(g_0)^2 = 0$$
 (9)

$$\theta'' + \Pr(f\theta' - f'\theta) - Q\theta + Nb\theta'\phi' + Nt(\theta')^{2} + \Pr Ec((f'')^{2} + (g_{0})^{2}) + \frac{\Pr EcM^{2}}{1 + m^{2}} (f'^{2} + g_{0}^{2}) = 0$$
(10)

$$\phi'' + Le(f\phi' - f'\phi) + (\frac{Nt}{Nb})\theta'' - (Le\gamma)\phi = 0$$
(11)

and the boundary conditions(6) are

$$f(0) = fw, f'(0) = 1, \theta(0) = 1, \phi(0) = 1, g(0) = 0$$
  
$$f'(\eta) \to 0, \theta(\eta) \to 0, \phi(\eta) \to 0, g(\eta) \to 0 \text{ as } \eta \to \infty$$
 (12)

Where  $fw = -v_0 / \sqrt{(cv/2L)}$  is the wall mass transfer parameter.

fw>0(vo<0) corresponds to mass suction and fw<0(vo>0) corresponds to mass injection.

The parameters occurring in (8)-(11) are defined as follows

$$M = \frac{2\sigma B_{o}^{2}L}{\rho_{f}c}e^{-\frac{x}{L}}, D^{-1} = \frac{kce^{\frac{c}{L}}}{2Lv}, Fs = \frac{2bL}{\sqrt{k}}, Pr = \frac{\mu C_{p}}{k_{f}}, v = \frac{\mu}{\rho}$$

$$Le = \frac{v}{D_{B}}, Nb = D_{B}\frac{(\rho C)_{p}(C_{w} - C_{w})}{(\rho C)_{f}}, Nt = \frac{D_{T}}{T_{w}}\frac{(\rho C)_{p}(T_{w} - T_{w})}{(\rho C)_{f}},$$

$$Q = \frac{Q_{H}(c/2L)}{e^{-\frac{x}{L}}}, R1 = \frac{4\Omega L}{U}, \gamma = \frac{k_{c}(c/2L)}{e^{-(\frac{x}{L})}}, U = ce^{\frac{x}{L}}$$

 $Q_{\rm H}=Q~(c~/~2L)e^{\frac{\dot{c}}{L}}$  is the non-uniform heat generation/absorption coefficient where Q>0 and Q<0 stand for

heat generating and absorption parameters respectively.R1 is the fluid rotational parameter,  $U=ce^{\frac{x}{L}}$  is the fluid velocity depending exponentially upon x.

The quantities of physical interest for this problem are the local skin friction due to linear motion(Cf),local skin friction due to rotation(Cg),local Nusselt number(Nux),local Sherwood number(Shx). These are defined as follows

$$C_{f} = \frac{\tau_{w}}{0.5\rho U_{w}^{2}} = \frac{\mu(\frac{\partial u}{\partial y})_{y=0}}{0.5\rho U_{w}^{2}} \Rightarrow C_{f} = \frac{1}{\sqrt{2R_{ex}}} f'(0)$$

$$C_{g} = -\frac{1}{\sqrt{2R_{ex}}} g(0), R_{ex} = u_{w}x/v$$

$$Nu_{x} = -\frac{x(\frac{\partial T}{\partial y})_{y=0}}{T_{w} - T_{\infty}} = -\sqrt{\frac{x R_{ex}}{L}} \theta'(0)$$

$$Sh_{x} = -\frac{x(\frac{\partial C}{\partial y})_{y=0}}{T_{w} - T_{\infty}} = -\sqrt{\frac{x R_{ex}}{L}} \phi'(0)$$



### 3. Comparison

Table 1. In the absence of convection (G=0, N=0), Chemical reaction ( $\gamma$ =0), Hall effects (m=0) the results are good agreement with Magyari and Keller (1999)

with Magyan and Keller (1999).											
Parameters				Magyari and Keller (1999) Results			Present Results				
M	D <sup>-1</sup>	fs	R	f''(0)	<i>g</i> ′(0)	$-\theta'(0)$	- <b>∮</b> ′(0)	f''(0)	g'(0)	$-\theta'(0)$	- <b>∮</b> ′(0)
0.5	1	0.5	0.01	-0.7914	-0.0365	0.3885	1.9228	-0.7917	-0.0366	0.3889	1.9229
0.7	1	0.5	0.01	-0.6559	-0.0564	0.4532	1.9655	-0.6551	-0.0560	0.4533	1.9655
1.0	1	0.5	0.01	-0.4363	-0.0919	0.5113	2.0118	-0.4366	-0.0916	0.5112	2.0119
0.5	2	0.5	0.01	-0.6206	-0.6185	0.4646	1.9735	-0.6207	-0.6190	0.4650	1.9736
0.5	3	0.5	0.01	-0.7361	-0.0443	0.4211	1.9459	-0.7362	-0.0444	0.4213	1.9457
0.5	1	1.0	0.01	-0.5789	-0.0366	0.4351	1.9816	-0.5792	-0.0369	0.4355	1.9822
0.5	1	1.2	0.01	-0.4814	-0.0237	0.4536	2.0035	-0.4816	-0.0239	0.4539	2.0037
0.5	1	0.5	0.03	-0.8049	-0.1353	0.3526	1.9230	-0.8060	-0.1355	0.3526	1.9232
0.5	1	0.5	0.05	-0.8283	-0.2177	0.3103	1.9151	-0.8281	-0.2179	0.3106	1.9113

#### 4. Results and discussion

The non-dimensional linear velocity  $f'(\eta)$ ,rotational velocity  $g(\eta)$ , temperature  $\theta(\eta)$  and nanoparticle volume fraction  $\phi(\eta)$  for various values of different parameters are exhibited in Figs. 2a-16a. To ensure the numerical accuracy, the values of f''(0) and  $f(\infty)$  by present method are compared with the results of Magyari and Keller (1999) in Table 1 without magnetic field (M=0),non-porous media(D-1=0,Fs=0) and having no rotational motion (R=0) and with nonporous stretching sheet(s=0) and those are found to be in excellent agreement. Thus, we are very much confident that the present results are accurate. The non-dimensional translational velocity  $f'(\eta)$ ,angular (rotational) velocity,  $g(\eta)$ ,temperature  $\theta(\eta)$  and nanoparticle volume fraction  $\phi(\eta)$  for values of Grashof number G are shown in Figs.2a-d. In the presence of mass fraction fw>0(vo<0), the translational velocity enhances and rotational velocity reduces with increase in G. This is due to the fact that the thickness of the momentum boundary layer increases with thermal buoyancy force which leads to an enhancement in  $f'(\eta)$  in the boundary layer. An increase in G results in an reduction of thermal boundary layer and increases the solutal boundary layer which give rise to a depreciation in temperature and an enhancement in nano particle volume fraction.

Figures 3a-d represent the variation of f',g  $,\theta$  and  $\phi$  with magnetic parameter M. It can be seen from the profiles that the translational velocity reduces while the rotational velocity enhances with increase in M. The increase of M leads to the increase of Lorentz force which is due to the interaction of magnetic and electric fields in the motion of an electrically conducting fluid. The weaker Lorentz force produces large resistance to the transport phenomena. The angular velocity enhances with M. Consequently, the momentum boundary layer thickness becomes thinner and the angular velocity boundary layer thickness becomes thicker. Also the temperature enhances and the nanoparticle volume fraction depreciates with M. This is due to the fact that the thickness of the thermal boundary layer increases and that of solutal boundary layer reduces for stronger magnetic field.

Figures 4a-d exhibits the variation of  $f,g,\theta$  and  $\phi$  withy Hall parameter(m).It is found that an increase in Hall parameter enhances the linear and rotational velocities, nanoparticle volume fraction and reduces the temperature. This is due to the fact that an increase in the Hall parameter (m) increases the thickness of the linear and rotational boundary layers and decreases the thickness of the thermal boundary layer. Also the solutal boundary layer thickness becomes thicker for higher values of Hall parameter.

Figures 5a-d show the variation of  $f',g',\theta'$  and  $\phi'$  with inverse Darcy parameter  $D^{-1}$ . The translational and angular velocities reduce with increase in  $D^{-1}$ . Thus lesser the permeability of the porous medium smaller the velocities in the boundary layer. The temperature increase and the nanoparticle volume fraction reduce with  $D^{-1}$ . Consequently the thermal boundary layer thickness becomes thicker and the nanoparticle volume faction boundary layer thickness becomes thinner for larger values of  $D^{-1}$ .

Figures 6a-d exhibit the variation of f',g , $\theta$  and  $\phi$  with rotation parameter (R). We find that the linear and angular velocity of the fluid decrease with increase in rotation parameter R. On the other hand, the temperature increases and the nanoparticle volume fraction reduces with increase in R. Consequently, velocity boundary thickness and angular velocity boundary layer thickness becomes thinner, and the thermal boundary layer thickness becomes thicker while the nanoparticle volume fraction boundary layer thickness becomes thinner for larger values of R.



Volume 2, Issue 12 May 2014

Figures 7a-d exhibit f', g,  $\theta$  and  $\phi$  with variation in heat source parameter Q. It can be seen from the profiles that in the presence of heat source the linear velocity, temperature decreases while the rotational velocity and nanoparticle volume fraction increases and a reversed effect is noticed in the presence of heat absorption. The is due to the fact that an increase in the fluid temperature causes more induced flow towards the plate through the thermal buoyancy effect and therefore the thickness of the thermal boundary layer is reducing for higher value of Q.

Figures 8a-b & 9a-d exhibit f'.a .0 and b with Brownian motion parameter Nb and thermophoretic parameter Nt. We notice from the profiles that the linear and angular velocities increase with increase in Nb and Nt in the boundary layer. Consequently the thickness of the linear and angular velocity boundary layers becomes thicker with increase in Nb and Nt. The temperature enhances with increase in Nb and Nt. while the nanoparticle volume fraction reduces with Nb and enhances with Nt. This is due to the fact that the thickness of the thermal boundary layer increases with increase in Nb and Nt. The thickness of the nanoparticle boundary layer decreases with Nb and increases with Nt.

Figures 10a-d show the variation of f', g,  $\theta$  and  $\phi$  with mass suction parameter fw. We find from the graphs that an increase in fw>0 enhances the linear velocity, and nanoparticle volume fraction, reduces the angular and temperature while a reversed effect is noticed in their behaviour with increase in injection parameter fw<0.

Figures 11a-d exhibit f',g ,θ and φ with Forchheimer parameter Fs. It can be seen from the profiles that the linear velocity and angular velocity of the fluid increase with increase of Forchheimer parameter Fs, except that in the region (2.0,4.0) the angular velocity experiences a depreciation with s. The temperature reduces while the nanoparticle volume fraction enhances with increase in Fs. Consequently, the thickness of the linear and angular velocity boundary layers become thicker .The thickness of the thermal boundary layer becomes thinner while the thickness of the nanoparticle volume fraction boundary layer becomes thicker for large values of Fs.

The effect of dissipation (Ec) on f', q,  $\theta$  and  $\phi$  is noticed from Figs.12a-d. Higher the dissipation energy larger the linear, angular velocities, temperature while smaller the nanoparticle volume fraction. Consequently, the thickness of the linear and angular velocity boundary layer becomes thicker with increase in Ec. The thermal boundary layer thickness becomes thicker while that of nanoparticle volume fraction becomes thinner with higher values of Ec.

Figures 13a-d represent the variation of f',g ,θ and φ withy Lewis number Le. We find that an increase in Le increases the thickness of linear, angular velocities, thermal and nanoparticle volume fraction.

Figures 15a-d and 16a-d demonstrate the variation of f',g ,θ and φ with chemical reaction parameter γ. The linear and angular velocities, nanoparticle volume fraction depreciate while the temperature enhances in the degenerating chemical reaction case while a reversed effect is noticed in the generating chemical reaction case. Consequently, the thickness of the boundary layers linear and angular velocities becomes thinner for γ>0 and becomes thicker for  $\gamma$ <0. The thickness of the thermal boundary layer increases, that of the nanoparticle volume fraction decreases for  $\gamma$ >0. while a reversed effect is noticed in their thickness for  $\gamma$ <0.

From figs. 14a-d we find that lesser the thermal diffusivity smaller the linear, angular velocities and temperature while larger the nanoparticle volume fraction in the boundary layer. We now discuss the variations of the physical quantities of engineering importance, that is, the local skin friction coefficient for linear velocity, Cf, local skin friction coefficient for rotational velocity Cg and the local Nusselt number Nux, local Sherwood number for different values of G, M, D<sup>-1</sup>, m, R, Nb, Nt, Ec, Le,  $\gamma$  and Pr. The quantities  $f''(0), g'(0), \theta'(0)$  and  $\phi'(0)$  related to local skin friction coefficient for linear velocity Cf, local skin friction coefficient for rotational velocity Cg, the local Nusselt Number Nux, local Sherwood number Shx are given in table.1 for various values of parameters.

702

Volume 2, Issue 12 May 2014



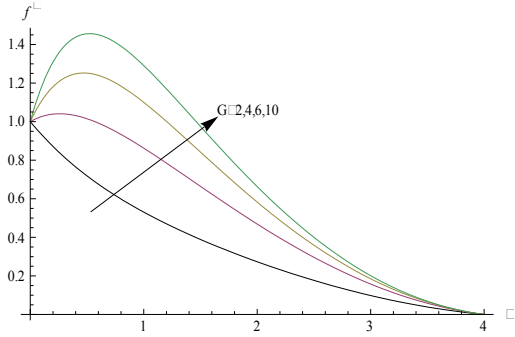


Fig.2a. Variation linear velocity(f') with G  $M=0.5, D-1=0.2, m=0.5, Nb=Nt=0.3, Pr=0.71, Q=0.5, fw=0.2 \\ M=0.5, D-1=0.2, m=0.5, Mb=Nt=0.3, Pr=0.71, Q=0.5, fw=0.2 \\ M=0.5, D-1=0.2, m=0.5, Mb=Nt=0.3, Pr=0.71, Q=0.5, fw=0.2 \\ M=0.5, D-1=0.2, m=0.5, Mb=Nt=0.3, Mb=Nt=0$ 

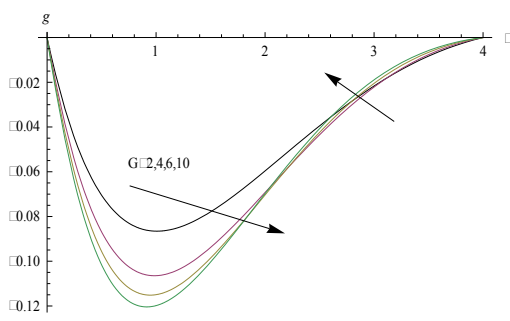


Fig.2b Variation of Rotational velocity(g) with G

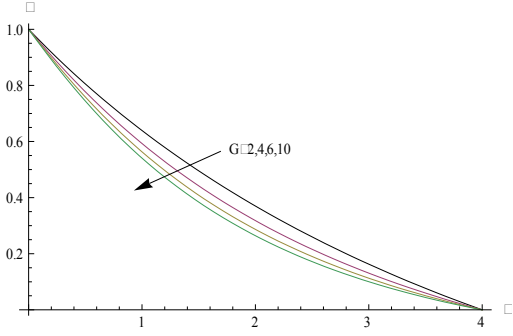


Fig.2c Variation of temperature(  $\boldsymbol{\theta}$  ) with  $\boldsymbol{G}$  $M=0.5, D-1=0.2, m=0.5, Nb=Nt=0.3, Pr=0.71, Q=0.5, fw=0.2; \ M=0.5, D-1=0.2, m=0.2, m=0.$ 

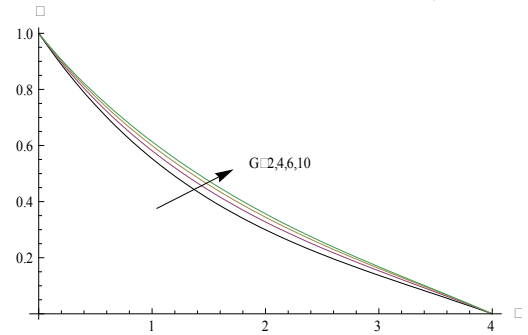


Fig.2d Variation Nanoparticle volume fraction( $\phi$ ) with G

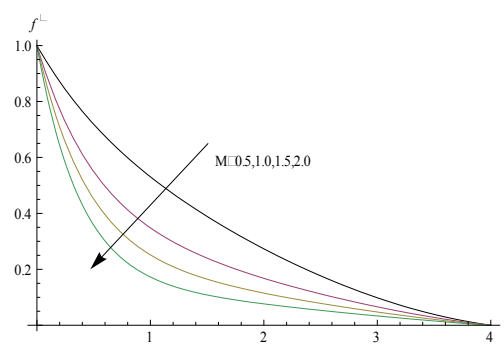


Fig.3a. Variation linear velocity(f') with M  $G=2,D-1=0.2,m=0.5,Nb=Nt=0.3,Pr=0.71,Q=0.5,fw=0.2;\ \ Q=0.5,fw=0.2,\ \ \gamma=0.5,Fs=0.2$ 

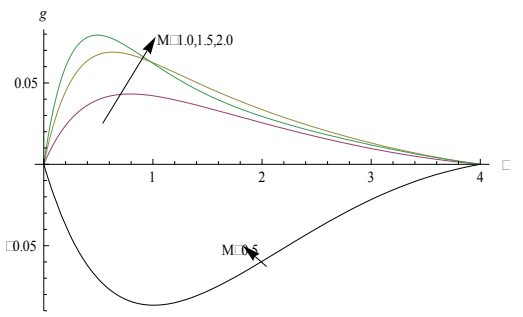
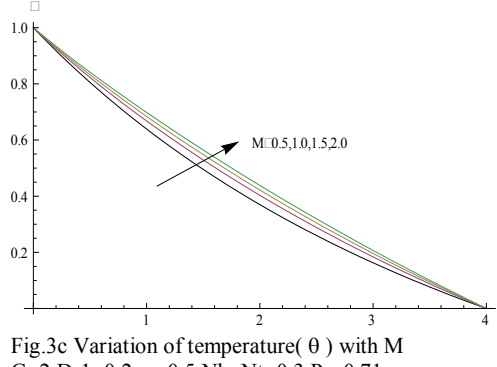


Fig.3b Variation of Rotational velocity(g) with M G=2,D-1=0.2,m=0.5,Nb=Nt=0.3,Pr=0.71,



G=2,D-1=0.2,m=0.5,Nb=Nt=0.3,Pr=0.71, Q=0.5,fw=0.2,Fs=0.2

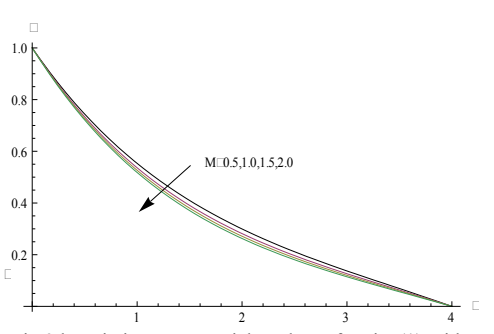


Fig.3d Variation Nanoparticle volume fraction(φ) with M G=2,D-1=0.2,m=0.5,Nb=Nt=0.3,Pr=0.71,Q=0.5,fw=0.2;Fs=0.2

Volume 2, Issue 12 May 2014



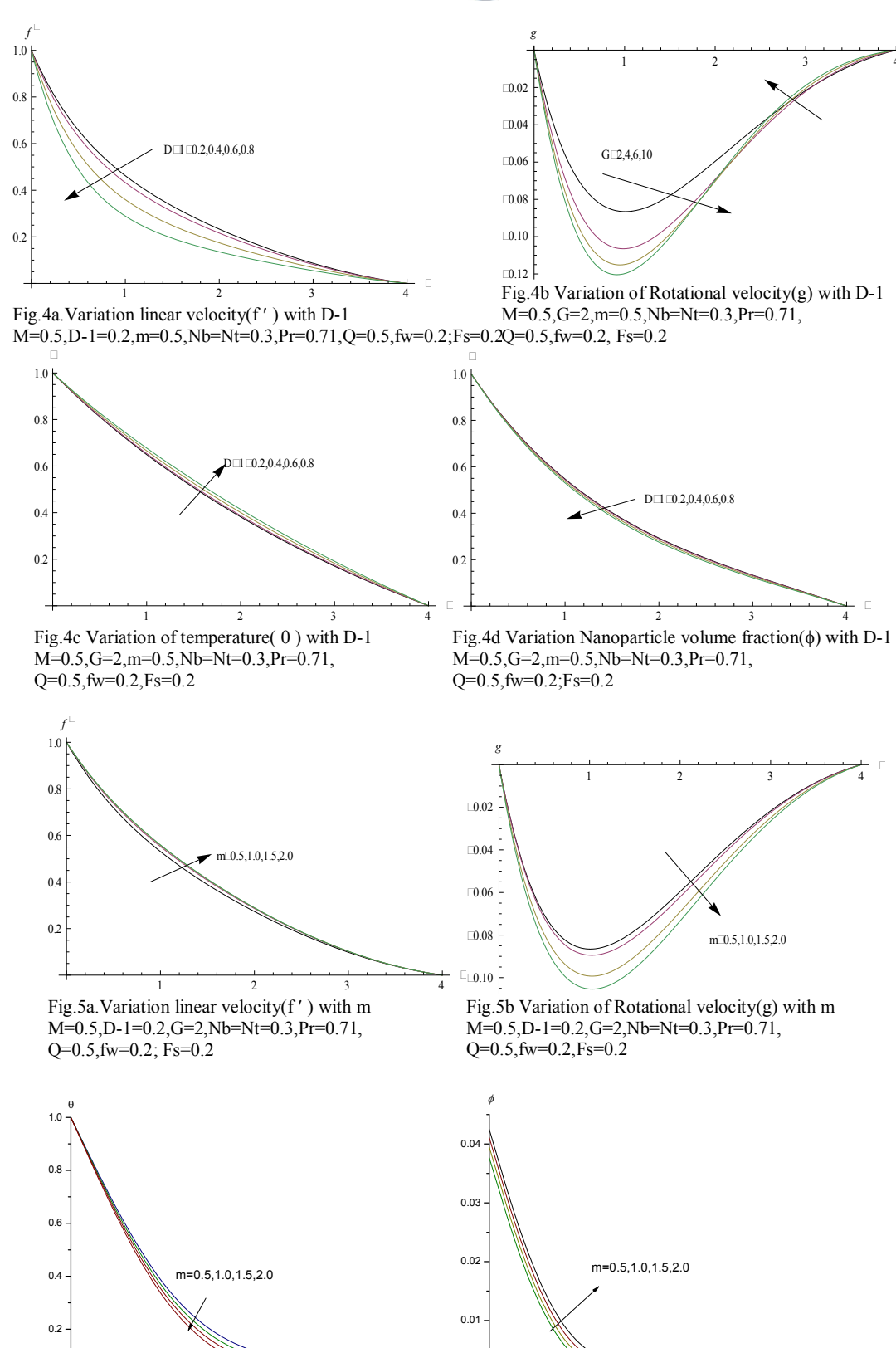


Fig.5c Variation of temperature( $\theta$ ) with m

Q=0.5,fw=0.2;Fs=0.2,  $\gamma$ =0.5

M=0.5,D-1=0.2,G=2,Nr=0.5,Nb=Nt=0.3,Pr=0.71,

0.0 -

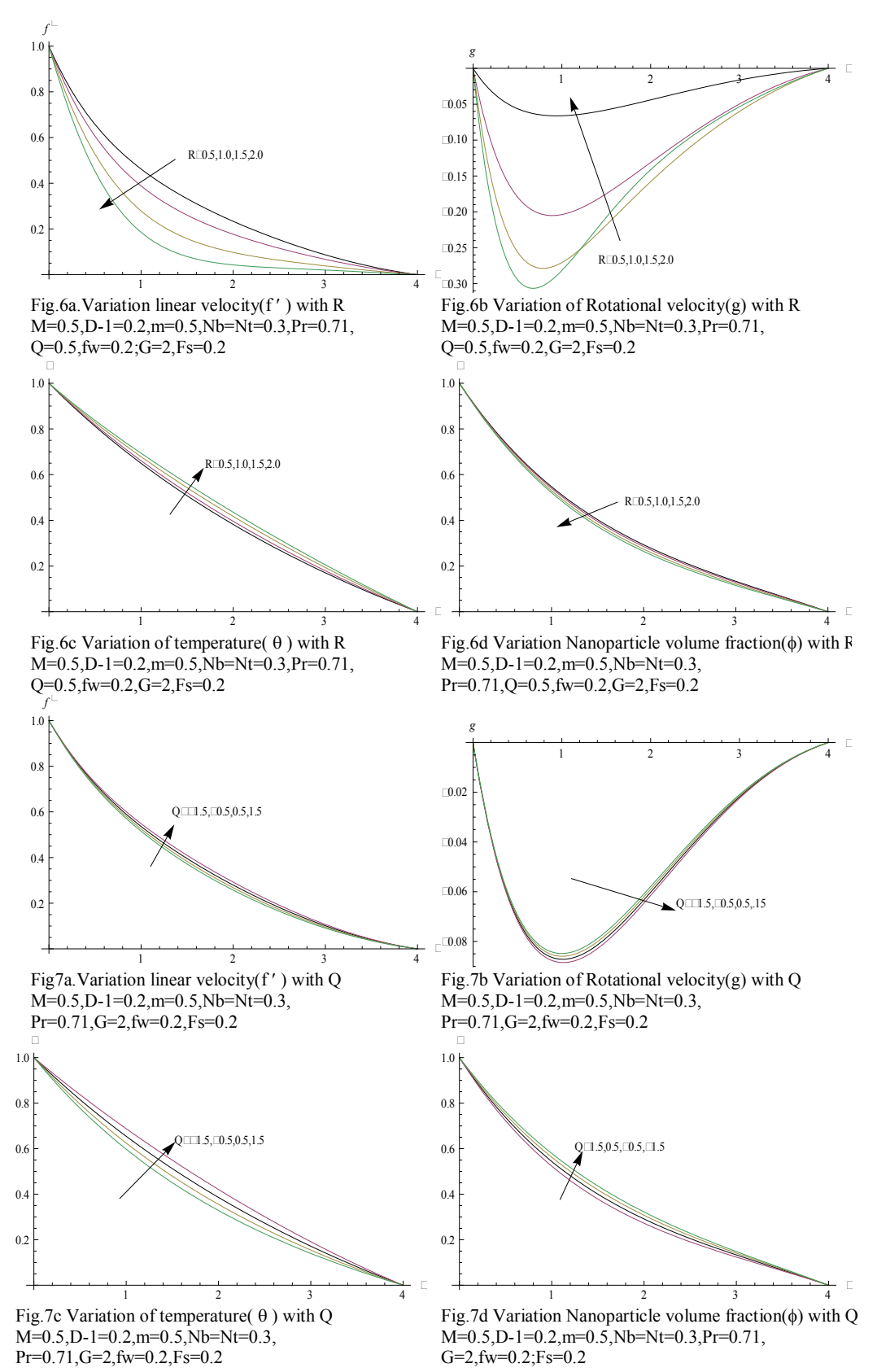
0.00

Fig.5d Variation Nanoparticle volume fraction(φ) with m

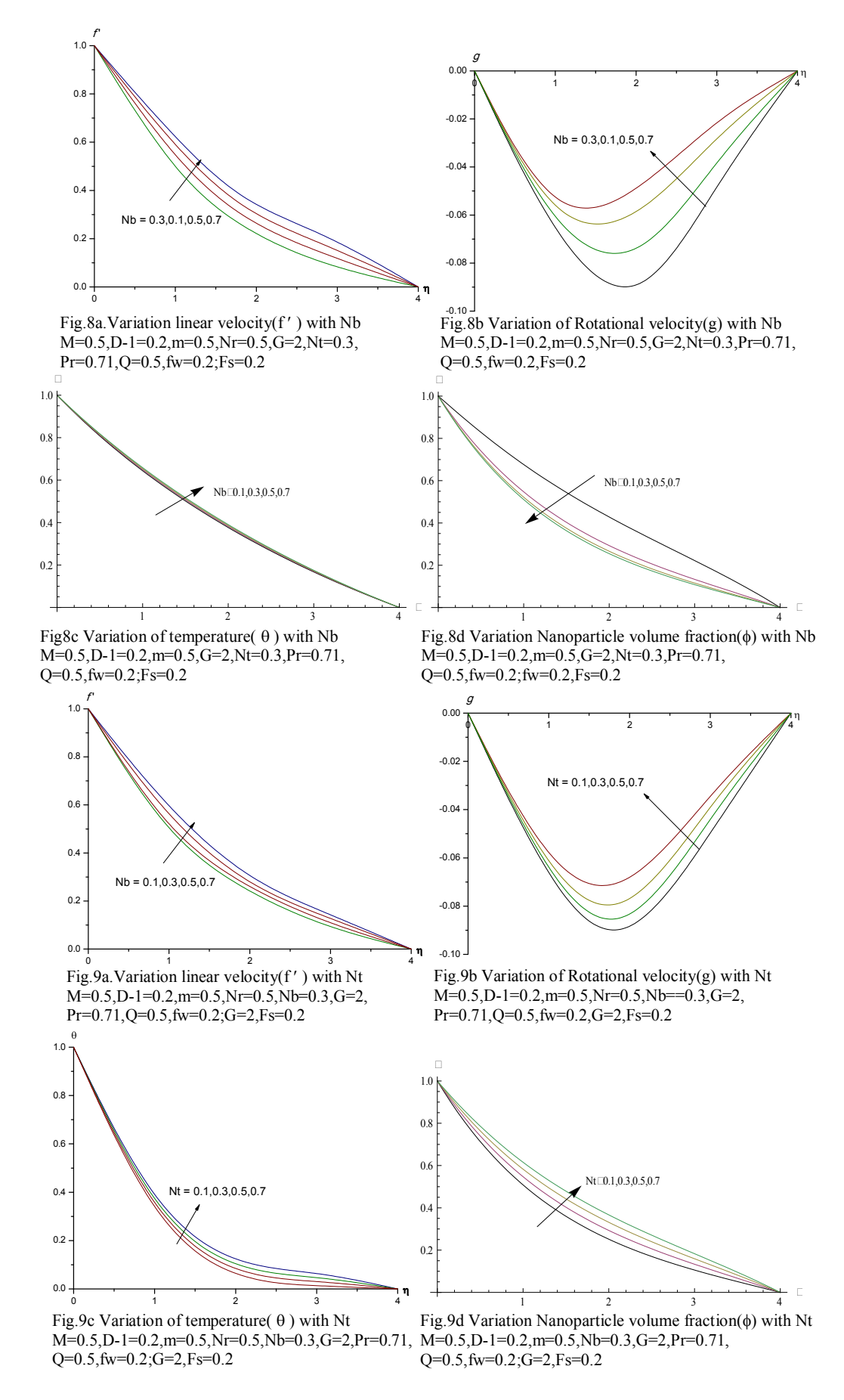
M=0.5,D-1=0.2,G=2,Nr=0.5,Nb=Nt=0.3,

 $Pr=0.71,Q=0.5,fw=0.2;Fs=0.2,\gamma=0.5,Fs=0.2$ 

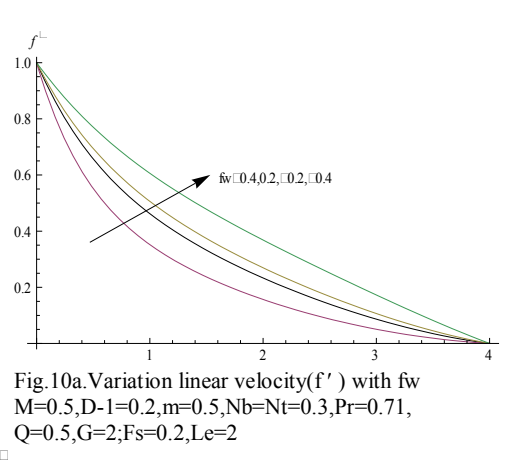












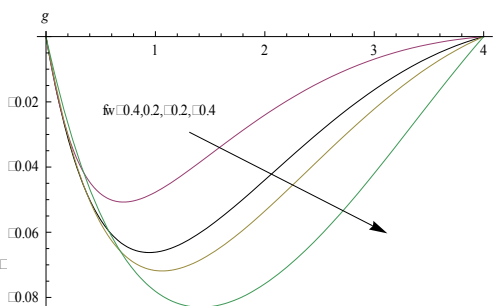
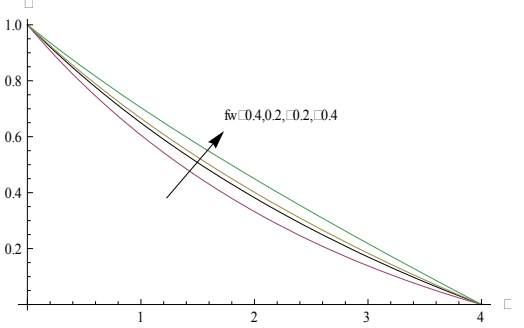
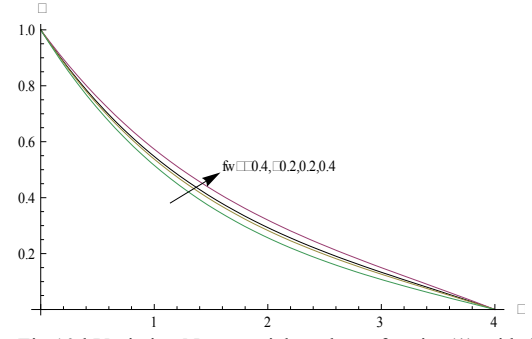
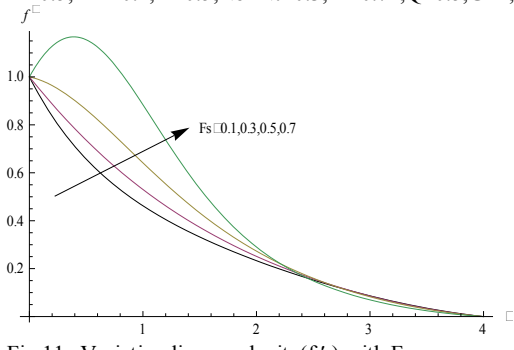


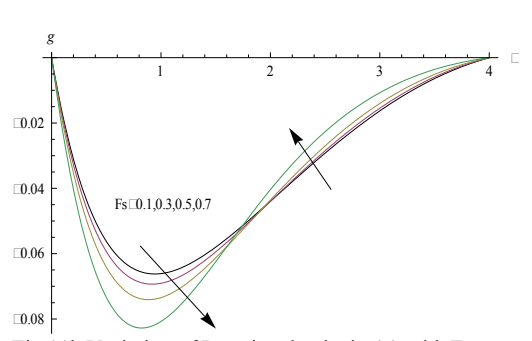
Fig. 10b Variation of Rotational velocity(g) with fw M=0.5,D-1=0.2,m=0.5,Nb=Nt=0.3,Pr=0.71,Q=0.5,G=2,Fs=0.2



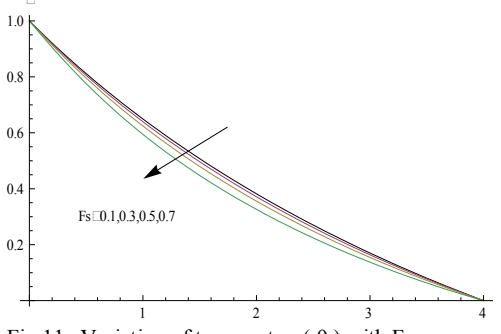


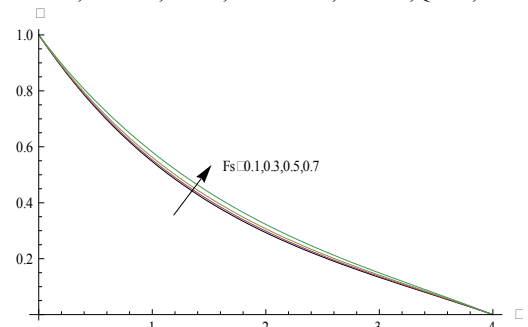
 $Fig. 10c\ Variation\ of\ temperature(\ \theta\ )\ with\ fw \\ M=0.5, D-1=0.2, m=0.5, Nb=Nt=0.3, Pr=0.71, Q=0.5, G=2; Fs=0.2\ M=0.5, D=0.5, D=0.5, Nb=Nt=0.3, Pr=0.71, Q=0.5, G=2; Fs=0.2\ M=0.5, D=0.5, D$ 





 $\label{eq:Fig.11a.Variation linear velocity} Fig. 11a. Variation of Rotational velocity(g) with Fs \\ M=0.5, D-1=0.2, \\ m=0.5, Nb=Nt=0.3, \\ Pr=0.71, Q=0.5, \\ fw=0.2; G=2M=0.5, \\ D-1=0.2, \\ m=0.5, Nb=Nt=0.3, \\ Pr=0.71, Q=0.5, \\ fw=0.2, \\ G=2M=0.5, \\ D-1=0.2, \\ m=0.5, \\ Nb=Nt=0.3, \\ Pr=0.71, \\ Q=0.5, \\ fw=0.2, \\ G=2M=0.5, \\ D-1=0.2, \\ m=0.5, \\ m=$ 





 $Fig. 11c\ Variation\ of\ temperature(\ \theta\ )\ with\ Fs\\ M=0.5, D-1=0.2, m=0.5, Nb=Nt=0.3, Pr=0.71, Q=0.5, fw=0.2; G=2\,M=0.5, D-1=0.2, m=0.5, D-1=0.2, m=0.5,$ 



Ec=0.2,0.4,0.6,0.8

0.2 0.0

Fig. 12a. Variation linear velocity(f') with Ec M=0.5,D-1=0.2,m=0.5,Nr=0.5,Nb=Nt=0.3,Pr=0.71, Q=0.5,fw=0.2;Fs=0.2,  $\gamma$ =0.5

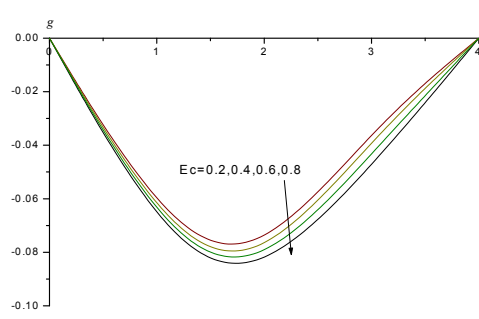


Fig. 12b Variation of Rotational velocity(g) with Ec M=0.5,D-1=0.2,m=0.5,Nr=0.5,Nb=Nt=0.3,Pr=0.71, Q=0.5, fw=0.2, Fs=0.2,  $\gamma$ =0.5

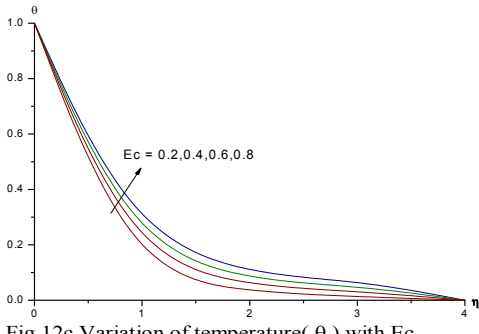


Fig.12c Variation of temperature(  $\boldsymbol{\theta}$  ) with Ec M=0.5,D-1=0.2,m=0.5,Nr=0.5,Nb=Nt=0.3,Pr=0.71, Q=0.5, fw=0.2; Fs=0.2,  $\gamma$ =0.5

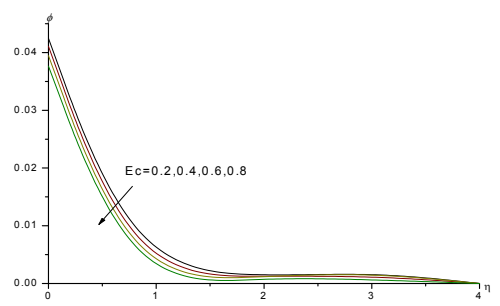


Fig.12d Variation Nanoparticle volume fraction( $\phi$ ) with Ec M=0.5,D-1=0.2,m=0.5,Nr=0.5,Nb=Nt=0.3,Pr=0.71, Q=0.5,fw=0.2;Fs=0.2,  $\gamma$ =0.5

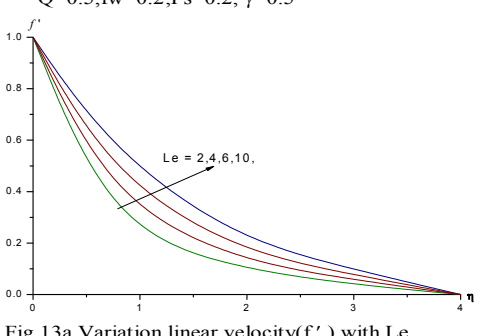


Fig.13a. Variation linear velocity(f') with Le M=0.5,D-1=0.2,m=0.5,Nr=0.5,Nb=Nt=0.3,Pr=0.71,Q=0.5, fw=0.2; Fs=0.2

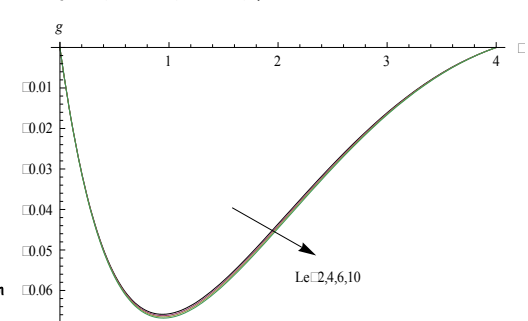
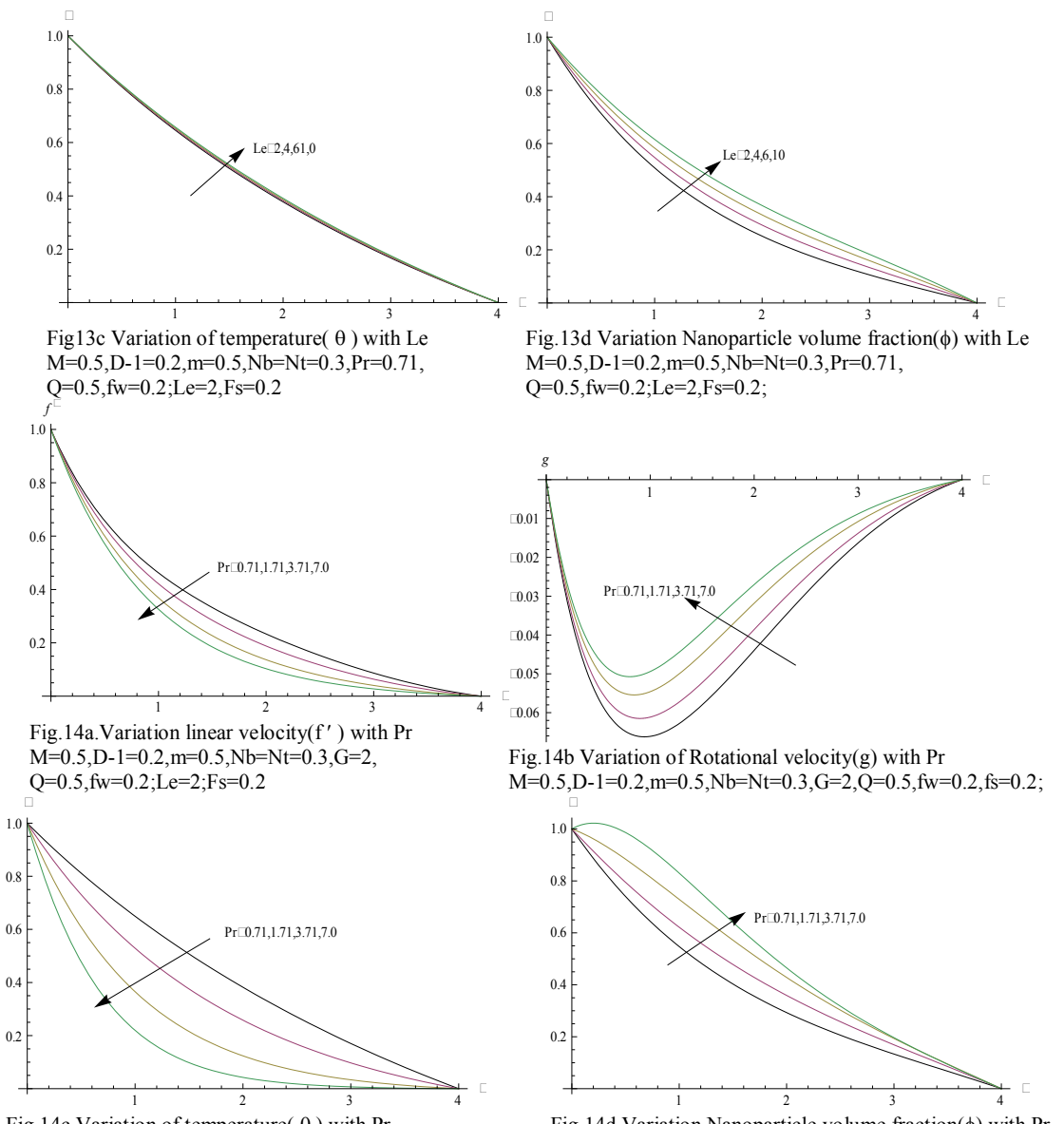
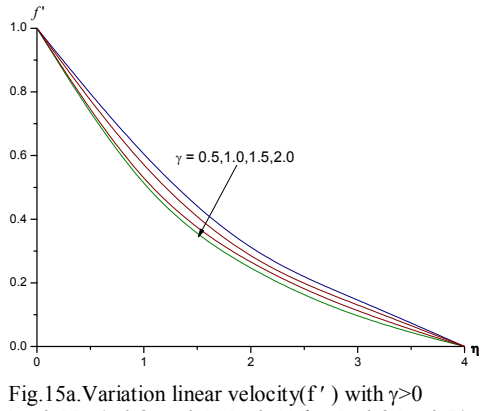


Fig.13b Variation of Rotational velocity(g) with Le M=0.5,D-1=0.2,m=0.5,Nb=Nt=0.3,Pr=0.71,Q=0.5,fw=0.2,Fs=0.2





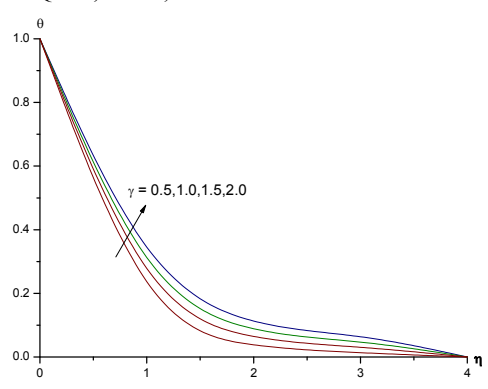




σ -0.02 -0.04 -0.06 -0.08

Fig.15a. Variation linear velocity(f ') with  $\gamma$ >0 M=0.5,D-1=0.2,m=0.5,Nr=0.5,Nb=Nt=0.3,Pr=0.71, Q=0.5,fw=0.2;Fs=0.2

Fig.15b Variation of Rotational velocity(g) with  $\gamma$ >0 M=0.5,D-1=0.2,m=0.5,Nr=0.5,Nb=Nt=0.3,Pr=0.71, Q=0.5,fw=0.2,Fs=0.2



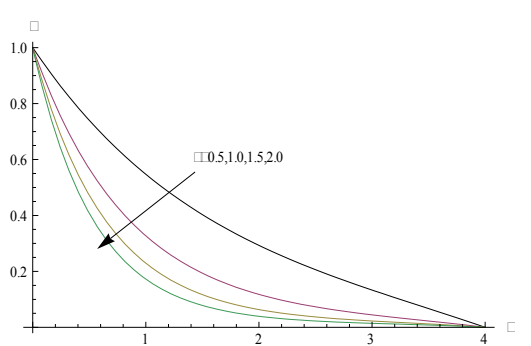
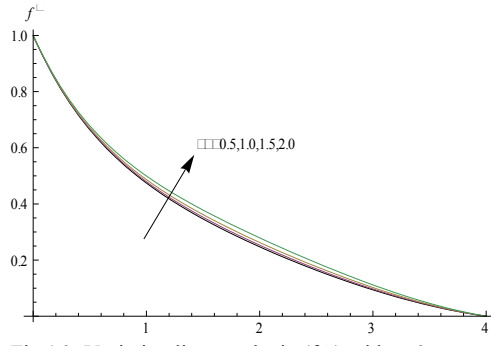


Fig.15c Variation of temperature(  $\theta$  ) with  $\gamma$ >0 M=0.5,D-1=0.2,m=0.5,Nr=0.5,Nb=Nt=0.3,Pr=0.71, Q=0.5,fw=0.2;Fs=0.2

Fig. 15d Variation Nanoparticle volume fraction( $\phi$ ) with  $\gamma$ >0 M=0.5,D-1=0.2,m=0.5,Nr=0.5,Nb=Nt=0.3,Pr=0.71, Q=0.5,fw=0.2;Fs=0.2



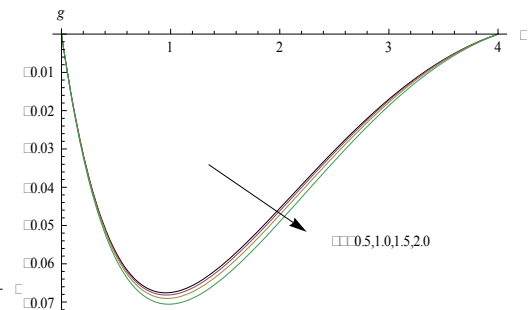
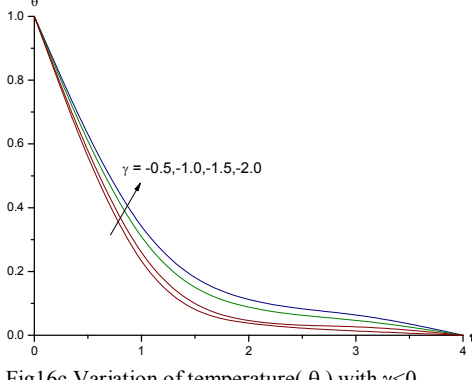


Fig.16a.Variation linear velocity(f  $^\prime$  ) with  $\gamma {<} 0$  M=0.5,D-1=0.2,m=0.5,Nr=0.5,Nb=Nt=0.3,Pr=0.71, Q=0.5,fw=0.2;Fs=0.2

Fig.16b Variation of Rotational velocity(g) with  $\gamma{<}0$  M=0.5,D-1=0.2,m=0.5,Nr=0.5,Nb=Nt=0.3,Pr=0.71, Q=0.5,fw=0.2,Fs=0.2



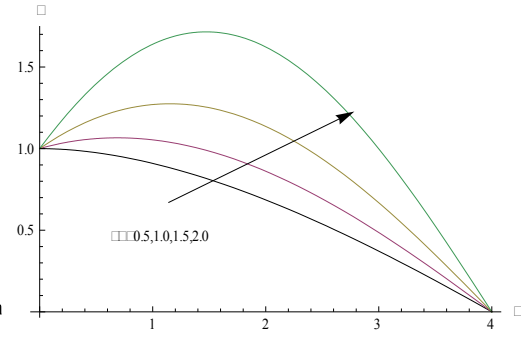


Fig16c Variation of temperature(  $\theta$  ) with  $\gamma$ <0 M=0.5,D-1=0.2,m=0.5,Nr=0.5,Nb=Nt=0.3,Pr=0.71, Q=0.5,fw=0.2;Fs=0.2

Fig.16d Variation Nanoparticle volume fraction( $\phi$ ) with  $\gamma$ <0 M=0.5,D-1=0.2,m=0.5,Nr=0.5,Nb=Nt=0.3,Pr=0.71, Q=0.5,fw=0.2;Fs=0.2



From Table 1 it is observed that the skin friction f"(0),g'(0) enhances with increase in G. The rate of heat and mass transfer at the wall enhance with G at the wall. An increase in magnetic parameter M enhances f" and reduces g',in view of larger momentum exerted on the wall with higher values of M. The magnetic parameter increases the wall heat and mass transfer rate . The effect of Hall parameter on the skin friction coefficient, heat transfer and Sherwood number is exactly same as that of magnetic parameter M. The porous parameter enhances f" and reduces q' on the wall. The rate of heat and mass transfer at the wall enhances with increase in porous parameter. When the molecular buoyancy force dominates over the thermal buoyancy force f" reduces and g' enhances, the rate of heat and mass transfer at the wall increases when the buoyancy forces are in the same direction. Higher the rotation parameter (R) larger the f" and g' at the wall, Nusselt number Nux and smaller Sherwood number Shx at η=0.In the presence of heat source f" decreases and g' increases while f" enhances and g' reduces with increase with that of strength of the heat absorption at the wall. The Nusselt number decreases and Sherwood number increases with increase in Q>0 while a reversed effect is noticed in their behaviour with increase in Q<0. The f" reduces and g" increases at the wall for an increase in Brownian motion parameter(Nb) and thermophoretic parameter(Nt) larger f",Nux, Shx and smaller g' at the wall. Higher the dissipation energy larger f", Nux and g', Shx at  $\eta$ =0. Increasing values of Pr enhances the wall heat and mass transfer. The skin friction component  $\tau x$  and Sherwood number (Sh) enhance, while  $\tau z$  reduces in both degenerating/generating chemical reaction cases. The Nusselt number (Nu) enhances in the degenerating case and reduces in the generating chemical reaction case. An increase in Forchheimer parameter (Fs) reduces the skin friction coefficients and enhances the rate of heat and mass transfer at the wall (Table 2).

Table 2. Skin Friction  $(\tau_x)$ , Nusslet number (Nu) and Sherwood Number (Sh) at  $\eta = 0$ 

Table 2. Skin Friction $(\tau_x)$ , Nusslet number (Nu) and Sherwood Number (Sh) at $\eta = 0$						
Para	ameter	τ <b>x</b> (0)	τz(0)	Nu(0)	Sh(0)	
G 2		-0.96665	-0.189257	0.50964	0.034058	
	4	-0.31447	-0.203866	1.18538	0.302151	
	6	0.156437	-0.211448	1.7338	0.486777	
	10	1.33142	-0.236274	2.32272	1.03666	
М	0.5	-0.96665	0.489257	0.50964	0.034058	
	1.0	-1.58521	0.36689	0.75146	0.134104	
	1.5	-1.95341	0.270072	0.96726	0.159948	
	2.0	-2.43722	0.232709	0.988894	0.164313	
m	0.5	-0.96664	-0.189257	0.50964	0.034058	
	1.0	-1.02161	-0.178571	0.99854	0.152294	
	1.5	-1.08183	-0.176862	1.44369	0.231682	
	2.0	-1.11999	-0.151428	1.84927	0.600451	
D-1	0.2	-0.96665	-0.189257	0.50964	0.034058	
	0.4	-1.22771	-0.157682	0.91818	0.214044	
	0.6	-1.46453	-0.134968	1.2787	0.293817	
	8.0	-1.63678	-0.121699	1.62952	0.406981	
Fs	0.2	-0.96665	-0.189257	0.50964	0.034058	
	0.4	-0.94938	-0.179232	1.00953	0.142988	
	0.6	-0.86628	-0.176017	1.49518	0.276691	
	0.8	-0.58034	-0.161687	1.99046	0.728933	
R	0.5	-0.96665	-0.189257	0.50964	0.534058	
	1.5	-1.15948	-0.591528	0.89976	0.225478	
	2.5	-1.35322	-0.893845	1.18768	0.12658	
	3.0	-1.51024	-1.01597	1.72587	0.097729	
Q	2	-0.70499	-0.228583	0.39709	0.610725	
	4	-0.68913	-0.230426	0.34271	0.649944	
	-2	-0.71933	-0.226891	0.44736	0.573979	
	-4	-0.72534	-0.226175	0.46881	0.558147	
Nb	0.2	-0.96641	-0.189486	0.56154	0.055437	
	0.4	-1.07141	-0.17659	0.9795	0.167003	
	0.6	-1.1396	-0.169212	1.34485	0.199046	
	8.0	-1.58786	-0.130498	1.82105	0.185934	
Nt	0.2	-0.97765	-0.18791	0.54079	0.144869	
	0.4	-1.07141	-0.17659	0.9795	0.167003	
	0.6	-1.12388	-0.171331	1.37043	0.750562	



Volume 2, Issue 12 May 2014

Table 2. Skin Friction  $(\tau_x)$ , Nusslet number (Nu) and Sherwood Number (Sh) at  $\eta = 0$ 

Parameter		τ <b>X</b> (0)	τ <b>z</b> (0)	Nu(0)	Sh(0)
	0.8	-1.51918	-0.136428	1.88326	2.40967
γ	0.5	-0.96664	-0.189257	0.509637	0.13405
	1.5	-1.08011	-0.175098	0.919957	0.86171
	-0.5	-1.00647	-0.196983	2.600864	1.66991
	-1.5	-1.19339	-0.154462	1.80558	2.62407
Ec	0.1	-0.96665	-0.189257	0.50964	0.13405
	0.3	-1.06776	-0.176903	0.94654	0.19726
	0.5	-1.13045	-0.170257	1.31107	0.11082
	0.7	-1.16916	-0.166871	1.61853	0.08493
Le	2	-0.96665	-0.189257	0.50964	0.13405
	4	-1.07141	-0.176594	0.97953	0.16703
	6	-1.14016	-0.169509	1.4206	0.21214
	10	-1.18452	-0.165805	1.82478	0.57864
Pr	0.71	-0.96665	-0.189257	0.50964	0.53405
	1.71	-1.07141	-0.176593	0.97953	0.16703
	3.71	-1.14016	-0.169509	1.4206	-0.212143
	7.0	-1.18452	-0.165805	1.82478	-0.578604

#### 4. Conclusion

We analyze the effect of Hall effects, heat sources, dissipation and chemical reaction on non-darcy convective heat and mass transfer flow of nanofluid past an exponentially stretching sheet. The nonlinear governing equation has been solved by Runge-kutta fourth order shooting technique. From the graphical and tabular representation we find that

- An increase in Hall parameter enhances the linear and rotational velocities, nanoparticle volume fraction and reduces the temperature.
- The linear and angular velocity of the fluid decrease with increase in rotation parameter R. On the other hand, the temperature increases and the nanoparticle volume fraction reduce with increase in R.
- In the presence of heat source the linear velocity, temperature decreases while the rotational velocity and nanoparticle volume fraction increases while a reversed effect is noticed in the presence of heat absorption
- Higher the dissipation energy larger the linear, angular velocities, temperature while smaller the nanoparticle volume fraction.
- The linear velocity and angular velocity of the fluid increase with increase of Forchheimer parameter Fs, except that in the region (2.0,4.0)the angular velocity experiences a depreciation with s. The temperature reduces while the nanoparticle volume fraction enhances with increase in Fs.
- $\bullet$  The skin friction component  $\tau x$  and Sherwood number (Sh) enhance, while  $\tau z$  reduces in both degenerating/generating chemical reaction cases. The Nusselt number (Nu) enhances in the degenerating case and reduces in the generating chemical reaction case.

### 5. References

- 1. Bhattacharya, K. and Pop, I. 2011. MHD boundary layer flow due to an exponentially shrinking sheet. Magnetohydrodynam. 47(4): 337-344.
- 2. Choi, S.U.S. 1995. Enhancing thermal conductivity of fluids with nanoparticles. Proceedings of the ASME International Mechanical Engineering Congress and Exposition, 66: pp.99-105.
- 3. Crane, L.J. 1970. Flow past a stretching plate. Zeitschrift für Angewandte Mathematik und Physik. ZAMP. 21(4): 645-647.
- 4. Ferdows, M., Khan, Md. and Alam, S.M. 2012. MHD mixed convective boundary layer flow of nanofluids through a porous medium due to an exponentially stretching sheet, Hindawi Publishing Corporation. Math. Prob. Engg. 15: 12-36.
- 5. Goyal, M. and Bhargava, R. 2013. Numerical solution of MHD viscoelastic Nanofluid flow over a stretching sheet with partial slip and heat source/sink, Hindawai Publishing Corporation, ISRN Nanotechnol. p.10211.
- 6. Hamad, M. and Ferdows, A.A.M. 2012. Similarity solutions to viscous flow and heat transfer of nanofluids over nonlinearly stretching sheet. Appl. Mathemat. Mech. 33(7): 923-930.
- 7. Ibrahim, S. M., Reddy, T.S. and Reddy, N. B. 2013. Radiation and mass transfer effects on MHD free convection flow of a micropolar fluid past a stretching surface embedded in a Non-Darcian porous medium with heat generation. ISRN Thermodynam. 2013: 534750.
- 8. Khan, Md. and Shakhnoath, Md. 2011. MHD radioactive boundary layer flow of an nanofluids past a stretching sheet. Proceedings of the International Conference on Mechanical Engineering and Renewable Energy 2011 (p. ICMERE2011), Chttagong, Bangladesh.

Volume 2, Issue 12 May 2014



713

- 9. Khan, W.A. and Pop, I. 2013. Buoyancy layer flow past a Wedge moving in a Nanofluid. Hindawi Publishing Corporation Mathematical Problems in Engineering, 2013, article ID 637285, 7.
- 10. Magyari, E. and Keller, B. 1999. Heat and mass transfer in the boundary layers on an exponentially stretching continuous surface. *J. Phy.* 32(5): 577-585.
- 11. Malvandi, A., Headyati, F. and Domairry, G. 2013. Stagnation point flow of a Nanofluid towards an exponentially stretching sheet with Non-Uniform heat generation/absorption, Hindawi Publishing Corporation. *J. Thermodynam.* Article ID 764827, 12.
- 12. Nandy, S.K. 2013. Analytical solution of MHD stagnation point flow and heat transfer of Casson fluid over a stretching sheet with partial slip, Hindawi Publishing Corporation *ISRN Thermodynam.* p.108264.
- 13. Njane, W.N. and Daniel, O. 2013. Combined effect of buoyancy force and Navier slip on MHD flow of a Nanofluid over a convectively heated vertical porous plate, Hindawi Publishing Corporation. *Scientific World.* p.725643.
- 14. Noghrehabadi, A., Ghalambaz, M. and Ghanbarzadeh, A. 2012. Heat transfer of magnetohydrodynamic viscous nanofluids over an isothermal stretching sheet. *J. Thermophy. Heat Transfer.* 26(4): 686-689.
- 15. Poornima, T. and Reddy, N.B. 2013. Radiation effects on MHD free convective boundary layer flow of nanofluids over a nonlinear stretching sheet. *Adv. Appl. Sci. Res.* 4(2): 190-202.
- 16. Shateyi, S. and Marewo, G.T. 2013. A new Numerical Approach of MH flow with Heat and Mass transfer for the UCM Fluid over a stretching surface in the presence of thermal radiation, Hindwai Publishing Corporation. Mathematical Problems in Engineering, 2013, article ID 670205,8 pages (2013)
- 17. Takhar, H. S., Chamkha, A. J. and Nath, G. 2003. Flow and heat transfer on a stretching surface in a rotating fluid with a magnetic field. *Int. J. Thermal Sci.* 42(1): 23-31.